# Distribution of mechanical stress in the Escherichia coli cell envelope

Hyea Hwang<sup>a,b,1</sup>, Nicolò Paracini<sup>c,1</sup>, Jerry M. Parks<sup>b</sup>, Jeremy H. Lakey<sup>c,\*</sup>, and James C. Gumbart<sup>d,\*</sup>

<sup>a</sup> School of Materials Science and Engineering, Georgia Institute of Technology, Atlanta, GA 30332
 <sup>b</sup> Biosciences Division, Oak Ridge National Laboratory, Oak Ridge, TN, USA <sup>c</sup> Centre for Bacterial
 Cell Biology, Institute for Cell and Molecular Biosciences, The Medical School, Newcastle University, Newcastle upon Tyne, NE2 4HH, United Kingdom <sup>d</sup> School of Physics, Georgia Institute of Technology, Atlanta, GA 30332

**Keywords:** membrane mechanics; area compressibility; turgor pressure; bacterial cell wall; lipopolysaccharides

Note to publisher. This manuscript has been authored by UT-Battelle, LLC under Contract No. DE-AC05-00OR22725 with the U.S. Department of Energy. The United States Government retains and the publisher, by accepting the article for publication, acknowledges that the United States Government retains a non-exclusive, paid-up, irrevocable, world-wide license to publish or reproduce the published form of this manuscript, or allow others to do so, for United States Government purposes. The Department of Energy will provide public access to these results of federally sponsored research in accordance with the DOE Public Access Plan (http://energy.gov/downloads/doe-public-access-plan).

<sup>&</sup>lt;sup>1</sup> These authors contributed equally to this work.

<sup>\*</sup> To whom correspondence should be addressed; Email: gumbart@physics.gatech.edu; Phone: 404-385-0797 and Email: jeremy.lakey@ncl.ac.uk; Phone: +44 (0) 191 208 8865

#### Abstract

The cell envelope in Gram-negative bacteria comprises two distinct membranes with a cell wall between them. There has been a growing interest in the mechanical adaptation of this cell envelope to the osmotic pressure (or turgor pressure), which is generated by the difference in the concentration of solutes between the cytoplasm and the external environment. However, it remains unexplored how the cell wall, the inner membrane (IM), and the outer membrane (OM) effectively protect the cell from this pressure by bearing the resulting surface tension, thus preventing the formation of inner membrane bulges, abnormal cell morphology, spheroplasts and cell lysis. In this study, we have used molecular dynamics (MD) simulations combined with experiments to resolve how and to what extent models of the IM, OM, and cell wall respond to changes in surface tension. We calculated the area compressibility modulus of all three components in simulations from tension-area isotherms. Experiments on monolayers mimicking individual leaflets of the IM and OM were also used to characterize their compressibility. While the membranes become softer as they expand, the cell wall exhibits significant strain stiffening at moderate to high tensions. We integrate these results into a model of the cell envelope in which the OM and cell wall share the tension at low turgor pressure (0.3 atm) but the tension in the cell wall dominates at high values (> 1 atm).

### Introduction

The Gram-negative bacterial cell envelope consists of two distinct membranes, inner and outer, along with a thin cell wall between them. The makeup of the inner, cytoplasmic membrane (IM) is broadly similar to the canonical picture of a membrane, being composed primarily of phospholipids. Unlike the IM, however, the outer membrane (OM) is highly asymmetric and has a completely different chemical composition [1]. The outer leaflet is composed primarily of lipopolysaccharide (LPS) contrasting with the inner leaflet of phospholipids. Whereas phospholipids have two aliphatic tails, these LPS molecules are large amphiphilic molecules with around six aliphatic tails, a core oligosaccharide head group, and in many variants, a repeating polysaccharide chain termed "O-antigen" that extends into the extracellular space [2]. Divalent cations promote ionic bridging between phosphate groups on the LPS core oligosaccharides, which creates a barrier to both hydrophobic and hydrophilic molecules [3].

Despite its name, the cell wall in Gram-negative bacteria is a single-layered ( $\sim$ 4-nm thick [4, 5]) porous mesh-like network that surrounds the cell. Although similar in composition, the cell wall in Gram-positive bacteria, which lack an OM, is roughly an order of magnitude thicker and is likely composed of multiple layers [6, 7]. The cell wall is composed of peptidoglycan, a contiguous network of strands of repeating units of the disaccharide N-acetyl glucosamine (GlcNAc)–N-acetyl muramic acid (MurNAc) that are cross-linked by short (5-10 residue) peptide side chains, all running roughly parallel to the cell surface between the IM and OM [8]. Disruption of the cell wall, e.g., by  $\beta$ -lactam antibiotics, causes inner membrane bulges, abnormal cell morphology, spheroplast formation, or cell lysis [9, 10].

The three components of the cell envelope (IM, OM and the cell wall) contribute to the mechanical stability of the cell and serve as barriers that permit selective diffusion and transport of small molecules. There has been a growing interest in the mechanical adaptation of the Gram-negative cell envelope to turgor pressure [11–16], which is generated by the difference in the concentration of solutes between the cytoplasm and the external environment. The turgor pressure under physiological conditions has been esti-

mated using several techniques, including chemical and mechanical measurements, with values varying by more than an order of magnitude, from 0.3 atm to 5 atm under normal conditions [17–20]. However, it has yet to be addressed how the surface tension, which protects against the expansion generated by the turgor pressure, is distributed between the cell wall and both membranes. Given the separation between the cell wall and both membranes observed in cryo-electron tomograms [4, 21, 22], stress transfer is unlikely to involve direct membrane-to-wall contact except, perhaps, in extreme conditions. However, the OM is often covalently connected to the cell wall in *Escherichia coli* by Braun's lipoprotein (Lpp), the most abundant protein in this species with at least 500,000 copies per cell (Fig. 1) [1, 22–24], and non-covalently connected through interactions with outermembrane proteins such as OmpA [25] and Pal [26]. While elimination of Lpp does not inhibit cell growth and division [27], elimination of both Lpp and OmpA causes *E. coli* cells to lyse unless electrolytes are added [28].

Here, we focus on resolving how the macroscopic properties of the bacterial cell envelope arise from the underlying features of its constituents. To correlate the structural characteristics of the membranes and cell wall with the mechanical resistance of the cell against the turgor pressure, it is necessary to understand the mechanical properties, e.g., elasticity, of each component. There have been a number of computational investigations into the mechanical properties of membranes. For example, pioneering simulation work by Tieleman et al. demonstrated that the application of a large mechanical pressure of -200 bar led to pore formation, i.e., a water channel, and irreversible rupture of a DPPC bilayer [30]. In another study, simulations were used to quantify the effect of membrane tension on a number of properties, such as area per lipid molecule, molecular volume, layer thickness, hydration thickness, lateral diffusion coefficient, and others, for a DOPC bilayer [31]. Many experiments probing various mechanical properties of phospholipid bilayers have also been carried out [32-35], including area compressibility [36, 37]. Recent simulations using the CHARMM36 force field [38], which is also used here, found good agreement with experiments for many of these mechanical properties, although not all; this is due in part to considerable uncertainty in the experimentally measured quantities [39].

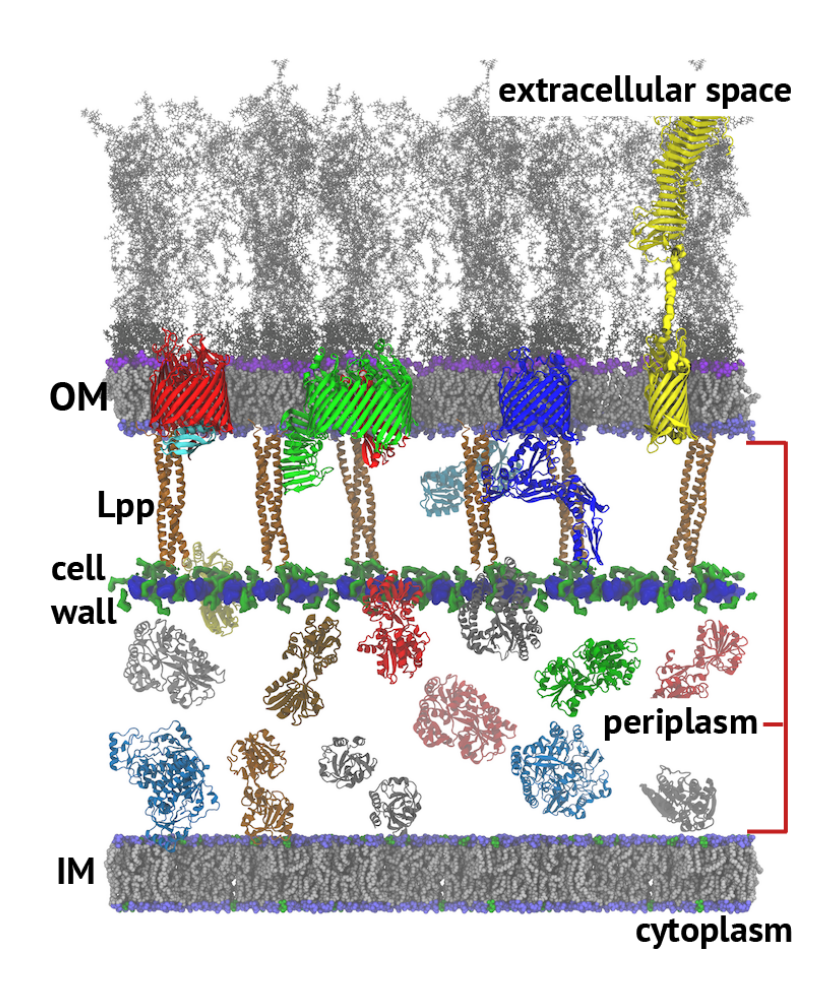


Figure 1: Model of the *E. coli* cell envelope. The two membranes, inner (IM) and outer (OM), along with the cell wall are labeled. The periplasm (between the membranes) is 240 Å thick. Proteins are shown to indicate scale but are of too low density [29]. Glycan strands of the cell wall are blue and peptide cross-links are green; Braun's lipoproteins (Lpp, tan) form triple-helices connecting the cell wall to the OM. From left to right, the OM proteins shown are BtuB, LptD/E, BamA, and pertactin.

In this paper, we carried out MD simulations of the individual components of the cell envelope (IM, OM, and the cell wall) with a variety of structural compositions, focusing on the effect of mechanical stress on each. As done in other MD simulation studies [31, 40–43], our simulations utilize an applied surface tension to mimic the effect of osmotic pressure. We determined area compressibilities of the simulated membranes and compared them with those from experiments on monolayers of identical compositions. To address how proteins may alter the stiffness of the membranes, we repeated the simulations with embedded, mechanically inert (i.e., not mechanosensitive) proteins. Lastly, we characterized the non-linear response of the cell wall to extreme stress in simulations, leading to

the observation of stress stiffening.

#### **Methods**

#### **Systems construction**

All-atom systems were generated for all membranes and cell wall models. All membranes were periodic, thus avoiding any edge effects that would otherwise arise due to exposed hydrophobic lipid tails. Similarly, the cell-wall system was also periodic with both peptides and glycan strands covalently linked across the periodic boundaries.

Inner membrane. Two models of the inner membrane (IM) were generated. One of the IMs was modeled as a mixed 75% POPE/25% POPG bilayer [44] (Fig. 2A). This model contained 270 lipids in each leaflet; the full system was 140K atoms in total, including water and 150 mM NaCl (177 Na<sup>+</sup> and 42 Cl<sup>-</sup> ions). The second IM model consisted of a mixture of six different kinds of saturated, unsaturated, and cyclic-moiety-containing lipids [45]. This complex membrane, referred to as Top6 (Fig. 2B), accurately reflects the diverse population of lipids within the *E. coli* cytoplasmic membrane. The model contained 296 PMPE, 80 POPE, 80 QMPE, 64 PMPG, 56 PSPG, and 48 OSPE lipids evenly distributed between the two leaflets; it was generated using the CHARMM-GUI membrane builder [46]. After the addition of water and 150 mM NaCl (189 Na<sup>+</sup> and 69 Cl<sup>-</sup> ions) to neutralize the system, the final system size was 150K atoms.

**Outer membrane.** An asymmetric outer membrane (OM) model was constructed with 75% POPE/25% POPG lipids for the inner leaflet and 100% LPS for the outer leaflet (Fig. 3A). This LPS is the rough form from *E. coli* K-12 (i.e., no O-antigen), also known as the RaLPS chemotype. The outer leaflet contained 108 LPS molecules and the inner leaflet had 261 POPE and 87 POPG lipids (phospholipid:LPS ratio of 3.22). After the addition of water and 530 Mg<sup>2+</sup>, 92 Ca<sup>2+</sup>, 168 Na<sup>+</sup>, and 168 Cl<sup>-</sup> ions, the asymmetric OM system had a total of 300K atoms. This LPS model was validated in our previous

simulations of the OM protein BtuB [47].

Addition of proteins. Biological membranes contain a substantial number of membrane proteins that are heterogeneously distributed [48–50]. A rough estimate from red blood cells is that ~25% of the membrane area is occupied by proteins [51], while computational modeling has been used to predict that the maximum growth rate is achieved at 25% and 42% area occupancy for OM and IM, respectively [49]. Therefore, we have also created membranes containing *E. coli* aquaporin Z (PDB ID: 1RC2; Fig. S2) in the IM and *E. coli* OmpF (PDB ID: 4GCP; Fig. S5) in the OM. For simplicity, the protein occupancy was set at 25% of the lateral area for all membranes.

**Cell wall.** The cell walls of Gram-negative bacteria consist of a thin layer of peptidogly-can. The glycan strands consist of alternating residues of  $\beta$ -1,4-linked N-acetylglucosamine (GlcNAc) and N-acetylmuramic acid (MurNAc), which is a uniform composition across all bacteria. In *E. coli*, a five-residue peptide chain is attached to the MurNAc, with the sequence L-Ala (1),  $\gamma$ -D-Glu (2), meso- $A_2$ pm (3), D-Ala (4), and D-Ala (5). In the mature molecule, the last D-Ala residue is lost when the peptide chain is cross-linked to the meso- $A_2$ pm residue of another peptide [8]. The system used in this study, which had an average glycan-strand length of 17 disaccharides and a cross-linking fraction of 50%, was taken from a previous study [5]. This cell wall model was fully solvated in explicit water with K<sup>+</sup> ions added to the solution to neutralize its high negative charge. The initial system size with water was 19 nm  $\times$  33 nm in area and contained 545K atoms. Once the cell wall patch was stretched to over 50% of its initial area, extra water was added, resulting in a system size of 829K atoms.

#### MD simulation

Molecular dynamics simulations were carried out with NAMD 2.12 [52] for the cell wall simulations and GROMACS 5.0.2 [53] for the membrane simulations, both using the CHARMM36 force field [38, 54]. All models were solvated with TIP3P water, and ions were

added to neutralize the system at a concentration of 150 mM NaCl. A constant temperature of 310 K = 37°C was maintained using Langevin dynamics (NAMD) or a Nosé-Hoover thermostat (GROMACS) [55, 56]; The pressure was coupled semi-isotropically with the Langevin piston (NAMD) [57] or the Parrinello-Rahman barostat (GROMACS) [58] at 1 atm and a coupling constant of 1.0 ps<sup>-1</sup>. The x- and y- directions were coupled independently from the z-direction. A 2-fs time step was used, and bonded and short-range nonbonded interactions were calculated every time step. Long-range electrostatic interactions were treated with the particle-mesh Ewald (PME) method [59], using a short-range cutoff of 1.2 nm; Lennard-Jones 6-12 (i.e., van der Waals) interactions were switched off between 1.0 to 1.2 nm using a force-based switching function. Buffered neighbor lists in GROMACS were maintained using the Verlet cutoff scheme. System setup, visualization, and analysis were performed with Visual Molecular Dynamics (VMD) [60].

### **Applied tension**

When a periodic system consists of several phases that are separated by surfaces parallel to the xy-plane, the surface tension and the z-component of the pressure can be coupled to a pressure bath. Pressure was kept constant for all simulation runs using the semi-isotropic Parrinello-Rahman pressure coupling algorithm, with the pressure set to 5-100 mN/m (note that 1 mN/m = 1 dyn/cm). A pressure of 1 bar was always applied in the normal direction. The average surface tension  $\gamma(t)$  can be calculated from the difference between the normal and the lateral pressure, resulting from the external pressure applied to the system as

$$\gamma(t) = \frac{1}{n} \int_0^{L_z} \left\{ P_{zz}(z,t) - \frac{P_{xx}(z,t) + P_{yy}(z,t)}{2} \right\} dz 
= \frac{L_z}{n} \left\{ P_{zz}(t) - \frac{P_{xx}(t) + P_{yy}(t)}{2} \right\}$$
(1)

where  $L_z$  is the length of the simulation box in the z-direction,  $P_{zz}$  is the pressure along the z axis,  $P_{xx}$  and  $P_{yy}$  are the lateral pressure in the x and y plane respectively, and n is the number of surfaces, which in this work is two.

To compute  $K_A$  for our systems, we ran a series of simulations in which increasingly

large negative lateral pressures were imposed to stretch the membrane. Starting from an equilibrated system, a tension of 5 mN/m was targeted, simulated, and then increased by 5-10 mN/m in each subsequent simulation. Performing the simulations in this manner allowed the bilayer to respond to the applied stress, maintaining quasi-equilibrium and, thus, minimizing the disruption to the system during each incremental increase.

#### **Experiments**

Pressure-area isotherms. Pressure-area isotherms were recorded on a Langmuir trough (NIMA, Coventry, UK) with a total surface area of 280 cm² and the surface tension measured using a paper Wilhelmy plate connected to a film balance. The trough was enclosed in a custom-built case saturated with water vapor to minimize evaporation of the subphase and the temperature controlled with a water bath connected to the trough. Phospholipids and *E. coli* polar lipid extract were dissolved in chloroform while RaLPS was dissolved in a mixture of phenol, chloroform and petroleum ether (2:5:8); all the solutions were at a concentration of 1 mg/ml. The aqueous subphase was buffered at pH 7.4 with 10 mM HEPES and contained 150 mM NaCl. The calcium concentration was controlled by adding calcium chloride to the subphase while 1 mM EDTA was used to remove any residual calcium in the Ca-free subphase. Lipids were spread on the buffered water surface using a Hamilton syringe and the solvent allowed to evaporate for 15 minutes before starting the experiments. Each isotherm was repeated three times by depositing monolayers on a freshly made subphase. The compression rate was 10 cm²/min.

### Results

The mechanical properties of biological membranes determine their thickness, their ability to compress, expand, and bend. The elastic modulus, or area compressibility ( $K_A$ ), characterizes the resistance of membrane to areal expansion or compression.  $K_A$  is calculated in MD simulations as the proportionality constant relating surface tension and

surface area according to the equation

$$K_{\rm A} = A_0 \left(\frac{\partial \gamma}{\partial A}\right)_T = \left(\frac{\Delta \gamma}{\Delta A/A_0}\right)_T \tag{2}$$

where A is the system area,  $A_0$  is the equilibrium area, T is the temperature (held constant at 37 °C), and  $\gamma$  is the surface tension. Because all of our simulations used periodic boundary conditions, the lateral dimensions of the box provide the surface area. Focusing on the linear regime of expansion,  $K_A$  was taken to be the slope of  $\gamma$  with respect to the fractional increase in area ( $\Delta A/A_0$ ).

In experiments, the surface pressure of a monolayer is measured as a function of the area per molecule in a Langmuir trough. From this relationship,  $K_A$  is calculated as

$$K_{\rm A} = -A_0 \left(\frac{\partial P}{\partial A_{\rm M}}\right)_T \tag{3}$$

where  $A_{\rm M}$  is the area per molecule (Å<sup>2</sup>), P is the surface pressure (mN/m), and T is the (constant) temperature (°C). We take  $A_0$  to be the value at  $P=35\,{\rm mN/m}$ , which is assumed to be the surface pressure of a tension-less membrane [61].

#### Determination of $K_A$ of the IM from simulations

Two models of the inner membrane (IM) were constructed as described in the Methods (Fig. 2). Briefly, one is a two-component mixture of a 3:1 ratio of POPE:POPG, as has been used in other studies [44, 45, 62]. The other is a mixture of six types of lipids meant to be an accurate representation of the *E. coli* IM, first developed by Pandit and Klauda [45], and referred to as Top6. Each targeted surface tension was simulated for 50 ns for both IM models. The area over time for the first tension simulated for each of the inner membrane models is given in Fig. S1, demonstrating that they reach an equilibrated state roughly halfway (25 ns) into the simulation period; similar behavior was observed at other tensions.

Averages of both the surface tension and the new area of the bilayer were calculated over the last 25 ns of each 50-ns simulation. Tension-area isotherms at 37 °C are plotted for both IMs in Fig. 2C, and  $K_A$  was determined according to Eq. 2. We note that each data point represents an individual simulation. The initial linear regime  $(\Delta A/A_0)$ 

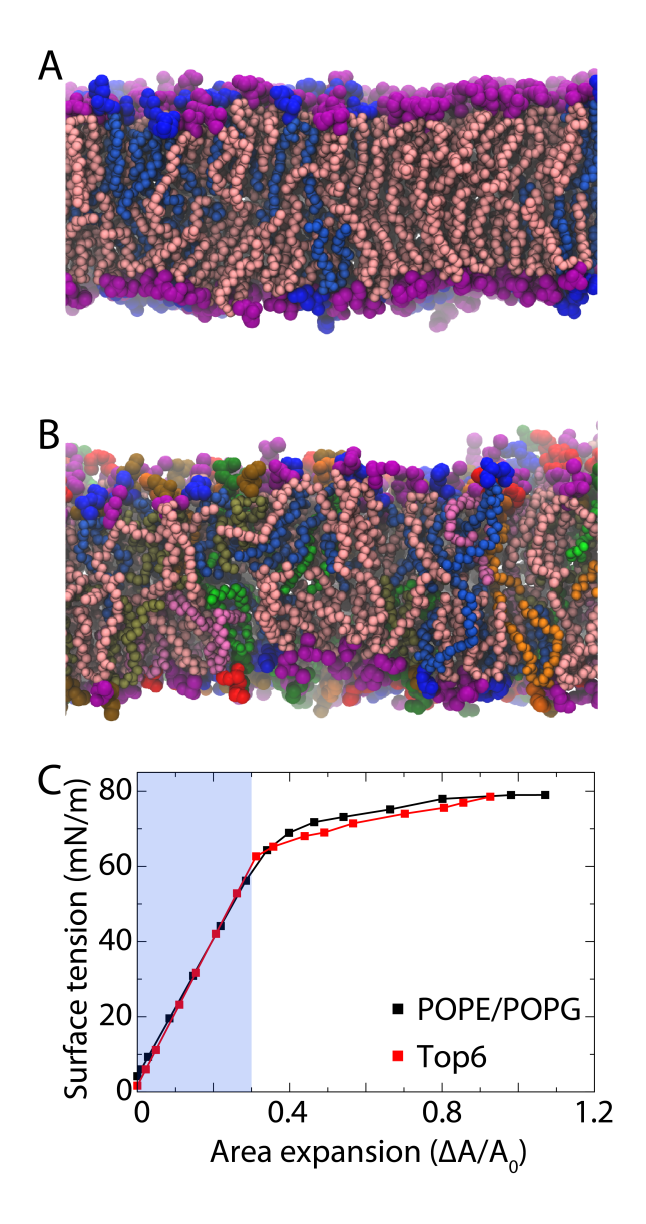


Figure 2: Simulation models of the inner membranes. (A) 3:1 POPE (pink tails/purple head groups):POPG (blue tails/blue head groups) bilayer. (B) Top6 bilayer (see Methods for composition). (C) Tension-area isotherms for inner-membrane models from simulation. The 3:1 POPE:POPG membrane is in black, and the Top6 membrane is in red.  $R^2$  values from the linear regression over the initial range ( $\Delta A/A_0$  between 0 and 0.35, shaded in blue) were 0.95 or higher for all IM models.

between 0 and 0.35) displays an elastic response of both membranes to tension. The calculated  $K_{\rm A}$  values are 182  $\pm$  21 and 195  $\pm$  23 mN/m for the POPE/POPG and Top6 membranes, respectively. Previous simulations of the same membranes produced much larger values of  $K_{\rm A}$ , specifically 250  $\pm$  40 mN/m for POPE/POPG and 340  $\pm$  40 mN/m

for Top6 [45]. The difference may be due to the method used; while we determined  $K_{\rm A}$  from tension-area isotherms, Pandit and Klauda calculated it from the area fluctuations of a zero-tension simulation [45]. The latter approach has been demonstrated to depend on the length of the simulation, with very short ones (< 1 ns) drastically overestimating  $K_{\rm A}$  by nearly an order of magnitude due to poor sampling of large fluctuations [63]. However, although the simulations of Pandit and Klauda were only 50 ns long (compared to ours, which were 50 ns per data point), more recent simulations of pure bilayers over 400 ns long produced  $K_{\rm A}$  values greater than 200 mN/m for a variety of pure membranes [39]. We also considered finite-size effects, as our membranes are  $4\times$  larger in area than those in Pandit and Klauda (312 lipids per leaflet vs. 78) [45]; however, Venable et al. concluded that there was no consistent dependence of  $K_{\rm A}$  on size [39]. Nonetheless, contributions from membrane undulations may be missed, particularly for small systems and/or those under applied tension [64].

To identify any effects of embedded proteins on mechanical properties of the membranes, we also simulated each IM model with an embedded aquaporin Z tetramer, which occupied 25% of the area (Fig. S2). Using the same protocol as for the pure membranes,  $K_{\rm A}$  was determined to be 199  $\pm$  25 mN/m for POPE/POPG and 218  $\pm$  26 mN/m for Top6, i.e., roughly 10% larger than the pure membranes (Fig. S3). This increase can be explained by the relative incompressibility of the protein compared to the membrane, which focuses all of the expansion on fewer lipids than in the pure membrane system.

#### Bilayer rupture by incremental tension and stress-softening

After an initial linear portion lasting up to about 35% of the ultimate load for both IMs, the stress-strain relationship enters a new regime in which large strains are observed for small increments of stress. Unlike a bulk material where the resistance to expansion comes from intermolecular bonds, the resistance to expansion in a bilayer is a result of non-polar interactions between the hydrophobic tails of each individual leaflet. The membrane displays an initial linear response at relatively low strain since the lipids in a fluid bilayer rearrange easily under the corresponding tension. However, once it gets

stretched further, the interactions between hydrophobic tails becomes weaker and the membrane undergoes a phase change (Fig. 2C).

We continued to apply incremental stretching to each membrane until it ruptured. Rupture occurs when a membrane reaches its critical lateral tension, which was found to be 79 mN/m and 78 mN/m for POPE/POPG and Top6 membranes, respectively (Fig. 2C). These values are in good agreement with other simulation results [30, 40, 65]. For example, a dipalmitoylphosphatidylcholine (DPPC) membrane withstood a surface tension of ~90 mN/m prior to rupture [65]. Another study also showed that an applied lateral pressure of -200 bar (~89 mN/m for their membrane) led to the formation and expansion of a water pore [40]. At the critical tension, water pores begin to form and destabilize the membrane, which causes the pores to grow further, resulting in bilayer rupture. Both membranes ruptured at approximately double their initial, relaxed area.

When proteins were embedded in the membranes, rupture occurred at slightly lower tensions compared to the pure membranes. This finding is consistent with the increase in  $K_A$  described in the previous section, which we attributed to the relative incompressibility of the protein. The location of the incipient water pore preceding rupture was in the middle of the membrane for both models, rather than between the protein and lipids, suggesting that the protein-lipid interactions are stronger than lipid-lipid interactions in these systems. See Figs. 2C and S4 for details of the rupture events.

We also found that both membranes exhibit a strong inelastic response, or stress-softening effect, at high tension. As a membrane is stretched further, the slope of the isotherm, which gives  $K_A$ , decreases (Fig. 2C). This strain-induced softening has been observed in viscoelastic materials with very weak intermolecular forces, and it results in a lower Young's modulus and higher failure strain compared to other materials [66, 67]. Using the last five data points before a water pore formed in the membranes, the  $K_A$  value was as low as 15 mN/m and 26 mN/m for POPE/POPG and Top6 membrane simulations, respectively.

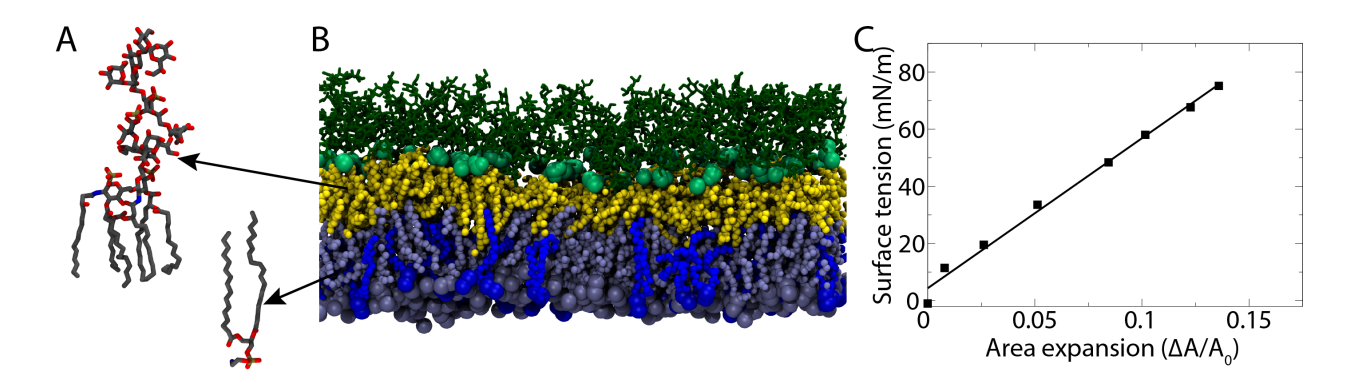


Figure 3: OM properties. (A) Single RaLPS molecule (left) and a POPE molecule (right). (B) Model of the OM. The hydrophobic region is shown as space-filling spheres with POPE in grey, POPG in blue, and lipid A of LPS in yellow. Phosphate groups of LPS are shown as large, light-green spheres, while phosphorus and nitrogen atoms of the inner leaflet lipids are colored grey or blue according to their type. The core oligosaccharides are shown as dark green sticks. (B) Tension-area isotherm for the OM model from simulations. The  $R^2$  value is 0.97. See Fig. S5 for the protein-containing OM.

#### Determination of $K_A$ of the OM from simulations

Similar to the calculations done for the IM models, we determined the area compressibility moduli for a pure outer membrane and for one with embedded proteins (Figs. 3B and S5, respectively). While the properties of the IM models stabilized relatively quickly (within 50 ns), the OM models were much slower to equilibrate. This finding was not unexpected, as the diffusion constant for LPS in the OM is two orders of magnitude lower than for phospholipids, due in part to the larger size of LPS as well as the numerous divalent ions bridging them [47]. To address this slow equilibration, simulations of the OM at each target surface tension were extended to 100 ns and their properties were measured over the last 50 ns.

Unlike the IM models, which showed a linear response to tension up to a 45% increase in area, the OM was very rigid. It was only 10% stretched at a tension of  $\sim$ 75 mN/m, which is the tension that caused rupture in the IM models. The calculated area compressibility modulus,  $K_{\rm A}=524\pm25\,{\rm mN/m}$ , is much higher than that found for the IM; this difference in  $K_{\rm A}$  agrees with another simulation study in which it was found that the outer membrane is more resistant than a phospholipid bilayer to rupturing via electroporation [68]. The rigidity and low mobility of the outer leaflet of the OM, composed purely of LPS molecules,

are mainly attributed to the divalent ( $Ca^{2+}$ ,  $Mg^{2+}$ ) ion-mediated cross-links, which form an electrostatic interaction network with the negatively charged  $PO_4^{2-}$  and  $COO^-$  groups of lipid A and the core sugars that make up LPS.

We also calculated the area compressibility modulus of the OM with embedded proteins, namely an OmpF trimer occupying 25% of the area. For this protein-membrane system, we obtained  $K_{\rm A}=528\pm25\,{\rm mN/m}$ , which is practically identical to that found for the pure OM (Fig. S6).

### Experimental determination of $K_A$ of the IM

To compare with the values of  $K_A$  from simulations, we also carried out experiments on monolayers representative of the simulated systems, namely a 3:1 POPE/POPG mixture and E. coli polar lipids, the latter being roughly equivalent to the Top6 membrane simulated. Pressure-area isotherms at 37 °C were determined in triplicate using a Langmuir trough with areas ranging from  $\sim$ 60-120 Å<sup>2</sup>/lipid (Fig. 4A). In both cases, the monolayers remained in the liquid-expanded (LE) phase and no plateau indicating a transition to the liquid-condensed (LC) phase was observed. A surface pressure of 35 mN/m has been determined to be equivalent to the internal pressure of a bilayer in a tension-free state and also the pressure at which various monolayer properties agree best with those measured in bilayers [61]. Thus, we compared the values of  $A_{\rm M}$  and  $K_{\rm A}$  at a pressure of 35 mN/m to the simulation results. At this pressure,  $A_{
m M}$  for the POPE/POPG mixture is 69.4  $\pm$  1.0  ${
m \AA}^2$ and for Top6 is  $63.0 \pm 1.9\,\mbox{Å}^2$ . Although the latter value is in good agreement with our simulated  $A_{\rm M}$  of 62 Å<sup>2</sup> for Top6, the former is quite different from the simulated value of 59 Å<sup>2</sup> for POPE/POPG. A similar discrepancy between experimental and simulated  $A_{
m M}$  of 3:1 POPE/POPG monolayers emerges from a comparison between independent published results. Although an MD study found an  $A_{\rm M}$  of 57.7 Å<sup>2</sup> [69], a separate investigation reported an experimental value of 65 Å<sup>2</sup> for the same lipid mixture under the conditions used here [70], suggesting a potential underestimation of the simulated result for this particular system.

Based on the surface pressure-area isotherms,  $K_{\rm A}$  of IM was calculated according to

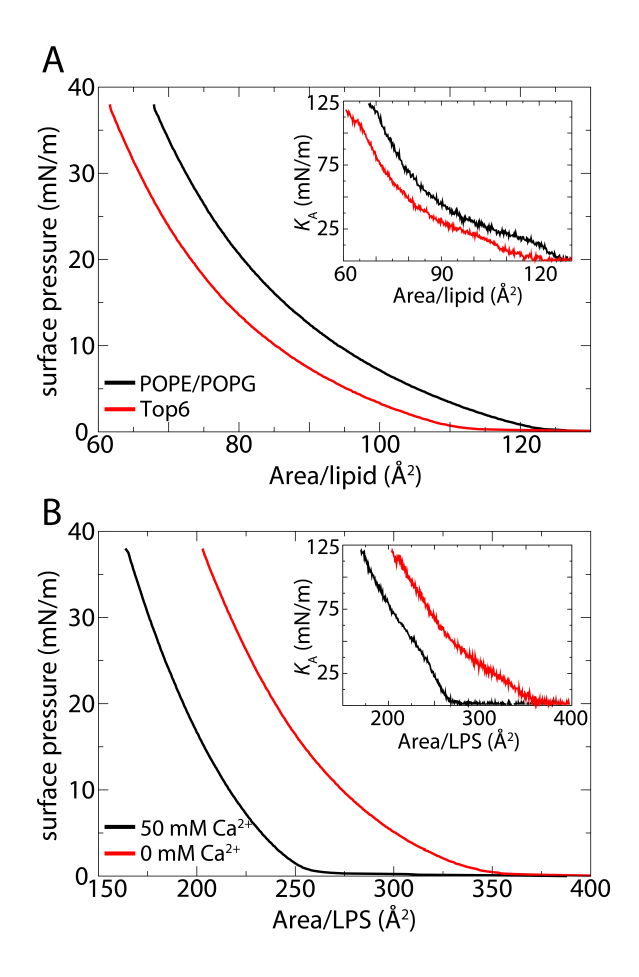


Figure 4: Surface pressure-area isotherms at 37 °C for monolayers from experiment. The inset in each panel shows  $K_A$  as a function of  $A_M$ . (A) IM models. The 3:1 POPE:POPG membrane is in black, and the Top6 membrane is in red. (B) OM model. Data for LPS with (black) and without (red) Ca<sup>2+</sup> are shown.

Eq. 3. For both IM models, a range of  $K_{\rm A}=0$  to 125 mN/m was observed. At a surface pressure of 35 mN/m,  $K_{\rm A}=123\pm3$  mN/m for POPE/POPG and 120  $\pm$  8 mN/m for Top6. As  $K_{\rm A}$  for a bilayer is just twice that of a monolayer [71], we conclude from experiments that  $K_{\rm A}$  is 246  $\pm$  6 mN/m for POPE/POPG and 240  $\pm$  16 mN/m for Top6 membranes under zero tension.

## Experimental determination of $K_{\rm A}$ of the OM

For the outer membrane, pressure-area isotherms were determined for the longest form of rough LPS (RaLPS), which was used to model the outer leaflet in the simulations (Fig. 3A), at Ca<sup>2+</sup> concentrations of 0 (Ca<sup>2+</sup>-free) and 50 mM (Ca<sup>2+</sup>-loaded). The latter

concentration, well above the physiological concentration, was employed in several previous studies to investigate the effects of Ca<sup>2+</sup> on LPS monolayers and is expected to saturate all Ca<sup>2+</sup> binding sites on LPS [72]. Unsurprisingly,  $A_{\rm M}$  was much higher when no Ca<sup>2+</sup> was present, due to the repulsion of the negatively charged groups on LPS, which are normally bridged by divalent cations, allowing for much tighter packing [73]. At a surface pressure of 35 mN/m,  $A_{\rm M}$  was 207.8  $\pm$  4.9 Å<sup>2</sup> for the Ca<sup>2+</sup>-free state and 168.6  $\pm$  1.4 Å<sup>2</sup> for the Ca<sup>2+</sup>-loaded state (Fig. 4B).

To our knowledge, these are the first RaLPS monolayers to be characterized at 37 °C. Thus, we also collected isotherms at 21°C (Fig. S7) to enable comparison with the published values for these systems. At this temperature and 35 mN/m, we obtained an  $A_{\rm M}$  of 187.9  $\pm$  1.3 Ų in the absence of Ca²+ which decreased to 156.2  $\pm$  3.2 Ų in the presence of 50 mM Ca²+. These values are in good agreement with those reported by previous studies, both differing by less than 10% [72].

The area compressibility varied from  $K_A = 0$  to 120 mN/m (Fig. 4B). Surprisingly, this compressibility of RaLPS is similar to the IM models, despite its apparent stiffness in the simulations. At a surface pressure of 35 mN/m,  $K_A$  for  $Ca^{2+}$ -loaded RaLPS was 120  $\pm$  8 mN/m and for  $Ca^{2+}$ -free RaLPS, it was 117  $\pm$  3 mN/m. The resistance to expansion in a bilayer is a result of the extra hydrophobic area exposed to water upon pulling the lipids apart. Therefore,  $K_A$  for a bilayer is taken to be twice that for a monolayer, as done in previous studies [61, 71]. In this work, because the OM is asymmetric, we combined  $K_A$  for the outer leaflet of LPS with  $K_A$  for the Top6 monolayer, which is representative of the inner leaflet of the OM, giving  $K_A = 237$  mN/m for the  $Ca^{2+}$ -loaded OM at zero tension.

### Determination of $K_A$ for the cell wall from simulations

The cell wall, a cross-linked polymer mesh of peptidoglycan (PG), is located in the periplasm between the IM and OM and is assumed to bear the majority of the turgor-pressure-induced stress [74]. The tensile elasticity, or Young's modulus, has been calculated previously from simulations for a specific arrangement of PG and was found to be anisotropic with  $E_{\rm circum.} = 66.3 \, \text{MPa}$  and  $E_{\rm lateral} = 17.5 \, \text{MPa}$  [5], in agreement with AFM experi-

ments [75]. The stiffer direction corresponds to the glycan strands encircling the cell circumferentially, and the more flexible direction corresponds to the peptide crosslinks that bridge the strands laterally [4, 76]. While previous simulations have focused on the elastic regime, we have performed additional simulations here to quantify the degree of strain stiffening, which has been observed for other biopolymer networks [66, 67, 77], including the cell wall [20].

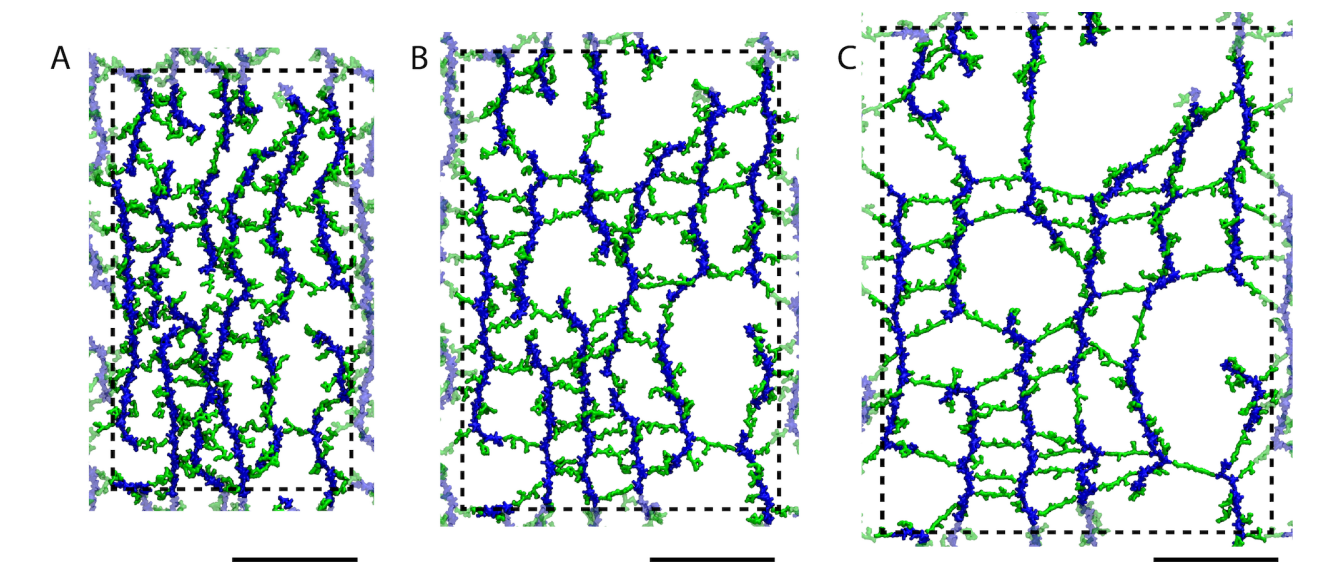


Figure 5: Representative states of the cell wall. Glycan chains are shown in blue and peptide cross-links in green; the cross-linked fraction of peptides is 50% [5]. The scale bar below each image is 10 nm. (A) Relaxed cell wall. (B) Cell wall stretched to  $1.5\times$  its original area. (C) Cell wall stretched to  $2\times$  its original area. Although covalent bonds cound not be broken in the simulations, we saw no change in average bond lengths in any simulations (Fig. S8B).

Rather than treating the two axes of the cell wall individually as done previously [5], multiple surface tensions were applied sequentially to a representative model patch of peptidoglycan and the resulting area change was monitored over a 10-ns simulation (see Methods). This patch, taken from a previous study [5], was first allowed to relax for 20 ns under zero applied tension, resulting in the configuration shown in Fig. 5A. Even with a very small applied surface tension of 6 mN/m, the area of the cell wall expanded to over 40% of its initial value (Fig. 6). Most of this expansion was due to the softer peptides, which expanded by  $\sim$ 30%, compared to the glycans, which expanded by only 10% (Fig. S8A). While extraordinarily soft at low tension, greater tensions applied to

the cell wall quickly revealed strain stiffening behavior as expected. For example, at the highest tension applied, more than  $11 \times$  the lowest tension ( $\sim$ 68 vs. 6 mN/m), the cell wall expanded by just over 100%, i.e., doubling its original area (Fig. 5C). This expansion arose from a 68% increase in the peptide direction and a 23% increase in the glycan direction. Although the peptidoglycan is apparently highly stretched at this expansion, it has not reached its elastic limit; average bond lengths in the glycan and peptide directions varied by 0.5% at most across all simulations (Fig. S8B).

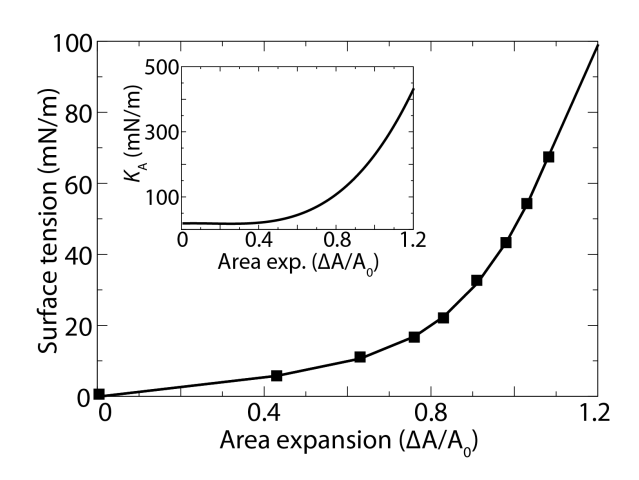


Figure 6: Tension-area isotherms for the cell wall model from simulation. The inset shows  $K_A$  as a function of the change in area due to applied tension. Standard deviation of the tension was  $\sim$ 3 mN/m, contributing to an error in  $K_A$  of at most 2%.

To compare with the values of  $K_{\rm A}$  from IM and OM simulations,  $K_{\rm A}$  of the cell wall,  $K_{\rm A}^{\rm CW}$ , was calculated according to Eq. 2, and the full isotherm is plotted in Fig. 6 (inset). While at low expansions, the compressibility is negligible, it quickly rises to over 200 mN/m at 100% expansion, i.e., comparable to those for the IM models from both simulations and experiments. In a living bacterial cell, the cell wall is strained, as upon cell lysis it shrinks by as much as 45% in area [78]. The cell wall shrinks mainly along the long (peptide) axis, forming wrinkles, with no change observed in the circumference in electron cryotomography (ECT) images [4]. Experiments in which E, Coli are subjected to hyperosmotic shock show an ability to shrink 33% in area, i.e., the cell wall  $\Delta A/A_0 = 0.5$  where  $A_0$  is the relaxed area [16, 79], and, in extreme cases, over 50% in area ( $\Delta A/A_0 = 1.25$ ) [16]. This range of  $\Delta A/A_0$  for our model of the cell wall predicts  $K_{\rm A}^{\rm CW}$  ranges from 29 to 500 mN/m

(Fig. 6). We also note that the spacing in our relaxed model between strands is 2-4 nm (Fig. 5A), in agreement with findings from AFM for cell wall fragments [76]; however, neither account for the ability of the continuous, intact cell wall to form wrinkles, which would shrink its area even further.

#### **Discussion**

Bacterial cells are very crowded due to the presence of metabolites and macromolecules, which can occupy a significant fraction of the total cellular volume (up to 30%) [80, 81]. When compared to the external environment, the cell interior usually possesses a higher concentration of solutes, resulting in turgor pressure. This results in a net water influx and cytoplasmic expansion which, when limited by the cell envelope comprising the IM, OM, and cell wall, results in turgor pressure. The turgor pressure in turn induces surface tension in the cell envelope. In this work, we have performed MD simulations of atomistic lipid bilayers and a model of the cell wall to gain insight into the distribution of surface tension between these three components of the cell envelope.  $K_A$  of each cell envelope component was determined from simulations and, for the IM and OM, compared to that derived from experimentally determined pressure-area isotherms.

The agreement between simulated and experimental values of  $K_{\rm A}$  was mixed. For both IM models, simulations underpredicted the experiments by 15-25%:  $K_{\rm A}$  for POPE/POPG was 182 mN/m in simulations and 238 mN/m in experiments, whereas for Top6, it was 195 mN/m in simulation and 226 mN/m in experiment. For the OM, simulations dramatically overpredicted the experimental result:  $K_{\rm A}$  was 524 mN/m in the simulation and only 233 mN/m in the experiments. It is surprising that our experimental compressibilities for phospholipid (113-119 mN/m) and LPS (110-120 mN/m) monolayers are nearly identical given their significantly different structures (Fig. 3A). Similar experiments on monolayers of other LPS variants have found a range of  $K_{\rm A}$  values, e.g., from 130 mN/m for *Salmonella enterica* ReLPS (an LPS variant shorter than RaLPS) [82] to 225 mN/m for *Pseudomonas aeruginosa* LPS [83]. X-ray studies of LPS at the air-water interface revealed the coexistence of crystalline domains and compressible disordered regions in the

monolayer, with the former prevailing at higher surface pressures [84]. The low compressibility obtained in the simulations might indicate that the in silico model of an LPS leaflet displays properties similar to the crystalline regions observed in the X-ray studies, possibly due the slow diffusion of LPS and the limited timescale of the simulation [47]. On the other hand, the presence of the more compressible disordered regions in the monolayer at the air-water interface would explain the lower  $K_A$  measured experimentally.

Additional simulations were performed with transmembrane proteins to determine whether their presence alters the stiffness of membranes. In both the IM and OM models, inclusion of proteins at a physiological protein density of 25% had at most a minor effect on  $K_A$ . Membrane proteins (AqpZ) in the IM made both POPE/POPG and Top6 membranes stiffer by  $\sim$ 10% (199 mN/m and 218 mN/m, respectively). This finding is consistent with coarse-grained simulations, which showed that the bending rigidity increased when aquaporin was in the membrane at a similar density [85]. In contrast, membrane proteins (OmpF) in the OM had practically no effect on  $K_A$ . The effect on  $K_A$  may be protein-dependent, as demonstrated previously for BtuB and OmpF, which have similar shapes but different effects on the rigidity of the membrane [85]. However, those simulations were performed in a phospholipid membrane that did not contain LPS, which clearly plays a role in the mechanical properties of simulated membranes, and also forms specific LPS-OmpF complexes [86].

If we assume that all three components of the cell envelope share the tension resulting from turgor pressure, we can calculate the fraction of tension each component bears based on their mechanical properties (see Supplemental Materials). From just a few inputs, including a turgor pressure of 1 atm and our measured  $K_A$  values for the IM and OM, we find that  $K_A^{\rm CW}=1386\,{\rm mN/m}$  and 1161 mN/m when using  $K_A^{\rm OM}$  of 233 mN/m (experiment) and 524 mN/m (MD simulation), respectively. Both calculated  $K_A^{\rm CW}$  values are nearly an order of magnitude higher than the value calculated from our simulations; furthermore, these values imply a tensile elasticity of 336 MPa and 281 MPa, which are also both an order of magnitude greater than practically all experimental estimates (see Ref. [87] and references therein). This discrepancy cannot easily be resolved by assuming a different Poisson's ratio for the membranes, and it only grows for larger values of the

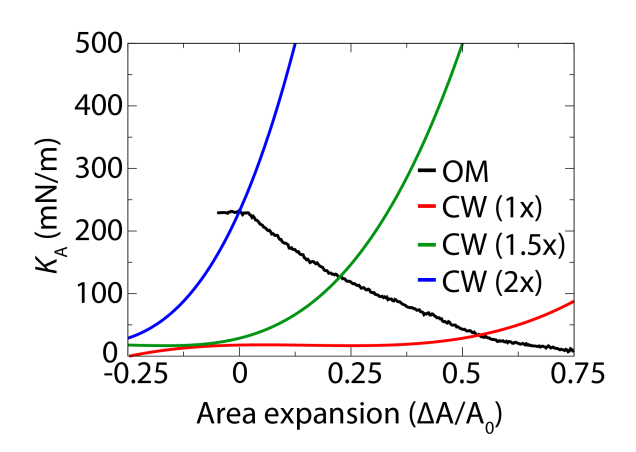


Figure 7: Strain-dependent area compressibility of the cell wall (CW) from simulations and the outer membrane (OM) from experiments. The cell wall is shown for three different assumed values of  $A_0$ . Due to strain stiffening, for a pre-strained cell wall,  $K_A$  rises drastically over a small range of  $\Delta A$ . See Fig. 5 for images of the cell wall at the same pre-strained values, i.e.,  $1 \times$ ,  $1.5 \times$ , and  $2 \times$  the fully relaxed area.

turgor pressure. Under these assumptions, the IM and OM each bear 10% of the tension and the cell wall bears 80%.

If, however, the turgor pressure is more modest, e.g., 0.3 atm as measured in some experiments in growth media [19, 20], we find  $K_{\rm A}^{\rm CW}=167\,{\rm mN/m}$  using the experimental  $K_{\rm A}^{\rm OM}=233\,{\rm mN/m}$ . This value is slightly less than that found in our simulations of the cell wall at  $2\times$  its relaxed area (Fig. 6). In this case, each of the three components, IM, OM, and cell wall, has the same amount of tension (one third of the total). If the IM does not participate directly in bearing the turgor pressure, then  $K_{\rm A}^{\rm CW}=342\,{\rm mN/m}$ , again using  $K_{\rm A}^{\rm OM}$  from experiment. This  $K_{\rm A}^{\rm CW}$  occurs at only 6% area expansion beyond the assumed  $2\times$  starting point (Fig. 7). In this case, the cell wall bears two-thirds of the tension and the OM bears the remaining one-third. Other possible distributions are presented in Table S1.

As O-antigen, which is usually present in pathogenic *E. coli* strains, is attached to the core oligosaccharide, one might assume that it will have an effect on the elasticity of the OM. Although the K-12 strain, which lacks O-antigens, was modeled here, a recent study found that the stiffness of *E. coli* cells increased when the O8 antigen, an electrically neutral linear poly-mannose, is present [16]. Thus, we expect that the OM in O-antigen-presenting bacteria would bear an even higher tension than that calculated above.

Recent work from Huang and colleagues also investigated the mechanical properties of the Gram-negative cell envelope [16]. Based on experiments in which the  $E.\ coli$  OM, cell wall, or both was compromised and then subjected to hyperosmotic shock, they concluded that the OM is an essential load-bearing element in addition to the cell wall, in agreement with our conclusions here, especially at low (0.3 atm) turgor pressure (Table S1). They also found that the cell wall length was between 25% and 50% expanded from its most relaxed state [16]. Using a simple model of  $E.\ coli$  as a cylinder of radius r, length 2r, and capped by hemispheres of radius r [88], this change in length translates to an area expansion of  $\sim$ 1.5-2.25 $\times$  the relaxed cell-wall area in the living cell. This area expansion is precisely the regime where we see overlap of the  $K_A$  values of the cell wall and OM. In particular, when the cell wall is twice its relaxed area,  $K_A^{CW}$  is identical to  $K_A^{OM}$  (Fig. 7), further supporting the conclusion of Rojas et al. that the OM and cell wall share the mechanical load due to the turgor pressure.

In conclusion, the high predicted  $K_{\rm A}^{\rm CW}$  values suggest that a turgor pressure of 1 atm is not feasible for the *E. coli* K-12 strain regardless of whether or not the IM plays a role in bearing it. At a turgor pressure of 0.3 atm, the cell wall can bear 0% – 65% of the pressure, depending on  $K_{\rm A}^{\rm OM}$  and whether or not the IM contributes. Assuming that the true  $K_{\rm A}$  of the OM is between our experimental and simulated values, it bears 35% – 78% of the 0.3-atm turgor pressure. Lastly, we demonstrated the inelastic behavior of the cell wall. When the turgor pressure rises due to an osmotic downshock, which is caused by a sudden decrease in the solute concentration outside of a cell, the distribution of surface tension will shift toward the cell wall bearing an increasingly large fraction of the tension, due to its ability to undergo strain stiffening, effectively increasing its  $K_{\rm A}$ , in agreement with previous measurements [20].

## **Acknowledgements**

This work was supported by a National Science Foundation Award (No. MCB-1452464) to J.C.G. and a US Department of Energy SCGSR fellowship to H.H. The SCGSR program is administered by the Oak Ridge Institute for Science and Education for the DOE

under contract number DE-SC0014664. J.M.P. was supported by National Institutes of Health grant R01-Al052293. N.P. was supported by a studentship jointly funded by the UK Science and Technology Facilities Council, Newcastle University and OJ-Bio Ltd. Computational resources were provided via the Extreme Science and Engineering Discovery Environment (XSEDE), which is supported by NSF Grant No. OCI-1053575. H.H. and J.C.G also thank James Sturgis for helpful discussions.

#### References

- [1] T. J. Silhavy, D. Kahne, S. Walker, The bacterial cell envelope, Cold Spring Harb. Perspect. Biol. 2 (2010) a000414.
- [2] C. R. Raetz, C. Whitfield, Lipopolysaccharide endotoxins, Annu. Rev. Biochem. 71 (2002) 635–700.
- [3] H. Nikaido, Molecular basis of bacterial outer membrane permeability revisited, Microbiol. Mol. Biol. Rev. 67 (2003) 593–656.
- [4] L. Gan, S. Chen, G. J. Jensen, Molecular organization of Gram-negative peptidoglycan, Proc. Natl. Acad. Sci. USA 105 (2008) 18953–18957.
- [5] J. C. Gumbart, M. Beeby, G. J. Jensen, B. Roux, *Escherichia coli* peptidoglycan structure and mechanics as predicted by atomic-scale simulations, PLoS Comput. Biol. 10 (2014) e1003475.
- [6] M. Beeby, J. C. Gumbart, B. Roux, G. J. Jensen, Architecture and assembly of the Gram-positive cell wall, Mol. Microbiol. 88 (2013) 664–672.
- [7] E. I. Tocheva, J. Lopez-Garrido, H. V. Hughes, J. Fredlund, E. Kuru, M. S. Vannieuwenhze, Y. V. Brun, K. Pogliano, G. J. Jensen, Peptidoglycan transformations during *Bacillus subtilis* sporulation, Mol. Microbiol. 88 (2013) 673–686.
- [8] W. Vollmer, D. Blanot, M. A. de Pedro, Peptidoglycan structure and architecture, FEMS Microbiol. Rev. 32 (2008) 149–167.
- [9] Z. Gitai, N. A. Dye, A. Reisenauer, M. Wachi, L. Shapiro, MreB actin-mediated segregation of a specific region of a bacterial chromosome, Cell 120 (2005) 329–341.
- [10] K. E. Daly, K. C. Huang, N. S. Wingreen, R. Mukhopadhyay, Mechanics of membrane bulging during cell-wall disruption in Gram-negative bacteria, Phys. Rev. E 83 (2011) 041922.

- [11] A. L. Koch, The biophysics of the Gram-negative periplasmic space, Crit. Rev. Microbiol. 24 (1998) 23–59.
- [12] W. Vollmer, S. J. Seligman, Architecture of peptidoglycan: more data and more models, Trends Microbiol. 18 (2010) 59–66.
- [13] H. Y. Jiang, S. X. Sun, Morphology, growth, and size limit of bacterial cells, Phys. Rev. Lett. 105 (2010) 028101.
- [14] L. Furchtgott, N. S. Wingreen, K. C. Huang, Mechanisms for maintaining cell shape in rod-shaped Gram-negative bacteria, Mol. Microbiol. 80 (2011) 340–353.
- [15] E. Rojas, J. A. Theriot, K. C. Huang, Response of *Escherichia coli* growth rate to osmotic shock, Proc. Natl. Acad. Sci. USA 111 (2014) 7807–7812.
- [16] E. R. Rojas, G. Billings, P. D. Odermatt, G. K. Auer, L. Zhu, A. Miguel, F. Chang, D. B. Weibel, J. A. Theriot, K. C. Huang, The outer membrane is an essential load-bearing element in Gram-negative bacteria, Nature (2018), in press.
- [17] D. S. Cayley, H. J. Guttman, M. T. Record Jr., Biophysical characterization of changes in amounts and activity of *Escherichia coli* cell and compartment water and turgor pressure in response to osmotic stress, Biophysics 78 (2000) 1748–1764.
- [18] M. Arnoldi, M. Fritz, E. BŁuerlein, M. Radmacher, E. Sackmann, A. Boulbitch, Bacterial turgor pressure can be measured by atomic force microscopy, Phys. Rev. E 62 (2000) 1034–1044.
- [19] X. Yao, J. Walter, S. Burke, S. Stewart, M. H. Jericho, D. Pink, R. Hunter, T. J. Beveridge, Atomic force microscopy and theoretical considerations of surface properties and turgor pressures of bacteria, Colloids Surfaces B: Biointerfaces 23 (2002) 213–230.
- [20] Y. Deng, M. Sun, J. W. Shaevitz, Direct measurement of cell wall stress stiffening and turgor pressure in live bacterial cells, Phys. Rev. Lett. 107 (2011) 158101.

- [21] V. R. F. Matias, A. Al-Amoudi, J. Dubocher, T. J. Beveridge, Cryo-transmission electron microscopy of frozen-hydrated sections of *Escherichia coli* and *Pseudomonas aeruginosa*, J. Bacteriol. 185 (2003) 6112–6118.
- [22] A. T. Asmar, J. L. Ferreira, E. J. Cohen, S. H. Cho, M. Beeby, K. T. Hughes, J. F. Collet, Communication across the bacterial cell envelope depends on the size of the periplasm, PLoS Biol. 15 (2017) e2004303.
- [23] V. Braun, Covalent lipoprotein from the outer membrane of *Escherichia coli*, Biochim. Biophys. Acta 415 (1975) 335–377.
- [24] W. Shu, J. Liu, H. Ji, M. Lu, Core structure of the outer membrane lipoprotein from *Escherichia coli* at 1.9 Å resolution, J. Mol. Biol. 299 (2000) 1101–1112.
- [25] F. Samsudin, M. L. Ortiz-Suarez, T. J. Piggot, P. J. Bond, S. Khalid, OmpA: A flexible clamp for bacterial cell wall attachment, Structure 24 (2016) 2227–2235.
- [26] E. Cascales, A. Bernadac, M. Gavioli, J.-C. Lazzaroni, R. Lloubes, Pal lipoprotein of *Escherichia coli* plays a major role in outer membrane integrity, J. Bacteriol. 184 (2002) 754–759.
- [27] H. Suzuki, Y. Nishimura, S. Yasuda, A. Nishimura, M. Yamada, Y. Hirota, Murein-lipoprotein of *Escherichia coli*: A protein involved in the stabilization of bacterial cell envelope, Molec. Gen. Genet. 167 (1978) 1–9.
- [28] I. Sonntag, H. Schwarz, Y. Hirota, U. Henning, Cell envelope and shape of Escherichia coli: multiple mutants missing the outer membrane lipoprotein and other major outer membrane proteins, J. Bacteriol. 136 (1978) 280–285.
- [29] K. A. Sochacki, I. A. Shkel, M. T. Record, J. C. Weisshaar, Protein diffusion in the periplasm of *E. coli* under osmotic stress, Biophys. J. 100 (2011) 22–31.
- [30] P. D. Tieleman, H. Leontiadou, A. E. Mark, S. J. Marrink, Simulation of pore formation in lipid bilayers by mechanical stress and electric fields, J. Am. Chem. Soc. 125 (2003) 6382–6383.

- [31] A. S. Reddy, D. T. Warshaviak, M. Chachisvilis, Effect of membrane tension on the physical properties of DOPC lipid bilayer membrane, Biochim. Biophys. Acta 1818 (2012) 2271–2281.
- [32] D. Needham, R. S. Nunn, Elastic deformation and failure of lipid bilayer membranes containing cholesterol, Biophys. J. 58 (1990) 997–1009.
- [33] K. Olbrich, W. Rawicz, D. Needham, E. Evans, Water permeability and mechanical strength of polyunsaturated lipid bilayers, Biophys. J. 79 (2000) 321–327.
- [34] W. Rawicz, K. C. Olbrich, T. McIntosh, D. Needham, E. Evans, Effect of chain length and unsaturation on elasticity of lipid bilayers, Biophys. J. 79 (2000) 328–339.
- [35] J. F. Nagle, S. Tristram-Nagle, Structure of lipid bilayers, Biochim. Biophys. Acta 1469 (2000) 159–195.
- [36] K. J. Tierney, D. E. Block, M. L. Longo, Elasticity and phase behavior of DPPC membrane modulated by cholesterol, ergosterol and ethanol, Biophys. J. 89 (2005) 2481–2493.
- [37] G. Popescu, T. Ikeda, K. Goda, C. A. B. Popescu, M. Laposata, Optical measurement of cell membrane tension, Phys. Rev. Lett. 97 (2006) 218101.
- [38] J. B. Klauda, R. M. Venable, J. A. Freites, J. W. O'Connor, D. J. Tobias, C. Mondragon-Ramirez, I. Vorobyov, A. D. MacKerell Jr., R. W. Pastor, Update of the CHARMM all-atom additive force field for lipids: validation on six lipid types, J. Phys. Chem. B 114 (2010) 7830–7843.
- [39] R. M. Venable, F. L. H. Brown, R. W. Pastor, Mechanical properties of lipid bilayers from molecular dynamics simulation, Chem. Phys. Lipids 192 (2015) 60–74.
- [40] H. Leontiadou, A. E. Mark, S. J. Marrink, Molecular dynamics simulations of hydrophilic pores in lipid bilayers, Biophys. J. 86 (2004) 2156–2164.
- [41] J. Neder, B. West, P. Nielaba, F. Schmid, Coarse-grained simulations of membranes under tension, J. Chem. Phys. 132 (2010) 115101.

- [42] H. S. Muddana, R. R. Gullapalli, E. Manias, P. J. Butler, Atomistic simulation of lipid and Dil dynamics in membrane bilayers under tension, Phys. Chem. Chem. Phys. 13 (2011) 1368–1378.
- [43] J. Y. Xie, G. H. Ding, M. Karttunen, Molecular dynamics simulations of lipid membranes with lateral force: Rupture and dynamic properties, Biochim. Biophys. Acta 1838 (2014) 994–1002.
- [44] J. Frauenfeld, J. Gumbart, E. O. van der Sluis, S. Funes, M. Gartmann, B. Beatrix, T. Mielke, O. Berninghausen, T. Becker, K. Schulten, R. Beckmann, Cryo-EM structure of the ribosome-SecYE complex in the membrane environment, Nat. Struct. Mol. Biol. 18 (2011) 614–621.
- [45] K. R. Pandit, J. B. Klauda, Membrane models of *E. coli* containing cyclic moieties in the aliphatic lipid chain, Biochim. Biophys. Acta 1818 (2012) 1205–1210.
- [46] E. L. Wu, X. Cheng, S. Jo, H. Rui, K. C. Song, E. Dávila-Contreras, Y. Qi, J. Lee, V. Monje-Galvan, R. M. Venable, J. B. Klauda, W. Im, CHARMM-GUI membrane builder toward realistic biological membrane simulations, J. Comput. Chem. 35 (2014) 1997–2004.
- [47] C. Balusek, J. C. Gumbart, Role of the native outer-membrane environment on the transporter BtuB, Biophys. J. 111 (2016) 1409–1417.
- [48] P. Rassam, N. A. Copeland, O. Birkholz, C. Toth, M. Chavent, A. L. Duncan, S. J. Cross, N. G. Housden, R. Kaminska, U. Seger, D. M. Quinn, T. J. Garrod, M. S. Sansom, J. Piehler, C. G. Baumann, C. Kleanthous, Supramolecular assemblies underpin turnover of outer membrane proteins in bacteria, Nature 523 (2015) 333–336.
- [49] J. K. Liu, E. J. O'Brien, J. A. Lerman, K. Zengler, B. O. Palsson, A. M. Feist, Reconstruction and modeling protein translocation and compartmentalization in *Escherichia coli* at the genome-scale, BMC Syst. Biol. 8 (2014) 110.

- [50] M. Linden, P. Sens, R. Phillips, Entropic tension in crowded membranes, PLoS Comput. Biol. 8 (2012) e1002431.
- [51] A. D. Dupuy, D. M. Engelman, Protein area occupancy at the center of the red blood cell membrane, Proc. Natl. Acad. Sci. U.S.A. 105 (2008) 2848–2852.
- [52] J. C. Phillips, R. Braun, W. Wang, J. Gumbart, E. Tajkhorshid, E. Villa, C. Chipot, R. D. Skeel, L. Kale, K. Schulten, Scalable molecular dynamics with NAMD, J. Comput. Chem. 26 (2005) 1781–1802.
- [53] M. J. Abraham, T. Murtola, R. Schulz, S. Páll, J. C. Smith, B. Hess, E. Lindahl, GROMACS: High performance molecular simulations through multi-level parallelism from laptops to supercomputers, SoftwareX 1-2 (2015) 19–25.
- [54] R. B. Best, J. Mittal, M. Feig, A. D. MacKerell, Jr., Inclusion of many-body effects in the additive CHARMM protein CMAP potential results in enhanced cooperativity of  $\alpha$ -helix and  $\beta$ -hairpin formation, Biophys. J. 103 (2012) 1045–1051.
- [55] S. Nosé, A unified formulation of the constant temperature?molecular dynamics methods, J. Chem. Phys. 81 (1984) 511.
- [56] Q. Hoover, Canonical dynamics: Equilibrium phase-space distributions, Phys. Rev. A 31 (1985) 1695?1697.
- [57] S. E. Feller, Y. H. Zhang, R. W. Pastor, B. R. Brooks, Constant pressure molecular dynamics simulations — The Langevin piston method, J. Chem. Phys. 103 (1995) 4613–4621.
- [58] M. Parrinello, A. Rahman, Polymorphic transitions in single crystals: A new molecular dynamics method, J. Appl. Phys. 52 (1981) 721–733.
- [59] T. A. Darden, D. M. York, L. G. Pedersen, Particle mesh Ewald: An *N* log *N* method for Ewald sums in large systems, J. Chem. Phys. 98 (1993) 10089–10092.
- [60] W. Humphrey, A. Dalke, K. Schulten, VMD Visual Molecular Dynamics, J. Mol. Graphics 14 (1996) 33–38.

- [61] D. Marsh, Lateral pressure in membranes, Biochim. Biophys. Acta 1286 (1996) 183– 223.
- [62] K. Murzyn, T. Rog, M. Pasenkiewicz-Gierula, Phosphatidylethanolamine-phosphatidylglycerol bilayer as a model of the inner bacterial membrane, Biophys. J. 88 (2005) 1091–1103.
- [63] S. E. Feller, R. W. Pastor, Constant surface tension simulations of lipid bilayers: The sensitivity of surface areas and compressibilities, J. Chem. Phys. 111 (1999) 1281– 1287.
- [64] E. Lindahl, O. Edholm, Spatial and energetic-entropic decomposition of surface tension in lipid bilayers from molecular dynamics simulations, J. Chem. Phys. 113 (2000) 3882–3893.
- [65] M. D. Tomasini, C. Rinaldi, M. S. Tomassone, Molecular dynamics simulations of rupture in lipid bilayers, Exp. Biol. Med 235 (2010) 181–188.
- [66] C. Storm, J. J. Pastore, F. C. MacKintosh, T. C. Lubensky, P. A. Janmey, Nonlinear elasticity in biological gels, Nature 435 (2005) 191–194.
- [67] K. A. Erk, K. J. Henderson, K. R. Shull, Strain stiffening in synthetic and biopolymer networks, Biomacromolecules 11 (2010) 1358–1363.
- [68] T. J. Piggot, D. A. Holdbrook, S. Khalid, Electroporation of the *E. coli* and *S. aureus* membranes: Molecular dynamics simulations of complex bacterial membranes, J. Phys. Chem. B 115 (2011) 13381–13388.
- [69] C. Hong, D. P. Tieleman, Y. Wang, Microsecond molecular dynamics simulations of lipid mixing, Langmuir 30 (2014) 11993–2001.
- [70] J. H. Borrell, O. Doménech, Critical temperature of 1-palmitoyl-2-oleoyl-sn-glycero-3-phosphoethanolamine monolayers and its possible biological relevance, J. Phys. Chem. B 121 (2017) 6882–6889.

- [71] S. Baoukina, L. Monticelli, S. J. Marrink, D. P. Tieleman, Pressure-area isotherm of a lipid monolayer from molecular dynamics simulations, Langmuir 23 (2007) 12617– 12623.
- [72] M. Herrmann, E. Schneck, T. Gutsmann, K. Brandenburg, M. Tanaka, Bacterial lipopolysaccharides form physically cross-linked, two-dimensional gels in the presence of divalent cations, Soft Mat. 11 (2015) 6037–6044.
- [73] E. Schneck, T. Schubert, O. V. Konovalov, B. E. Quinn, T. Gutsmann, K. Brandenburg, R. G. Oliveira, D. A. Pink, M. Tanaka, Quantitative determination of ion distributions in bacterial lipopolysaccharide membranes by grazing-incidence X-ray fluorescence, Proc. Natl. Acad. Sci. U.S.A. 107 (2010) 9147–9151.
- [74] J. V. Höltje, Growth of the stress-bearing and shape-maintaining murein sacculus of *Escherichia coli*, Microbiol. Mol. Biol. Rev. 62 (1998) 181–203.
- [75] X. Yao, M. Jericho, D. Pink, T. Beveridge, Thickness and elasticity of Gram-negative murein sacculi measured by atomic force microscopy, J. Bacteriol. 181 (1999) 6865– 6875.
- [76] R. D. Turner, S. Mesnage, J. K. Hobbs, S. J. Foster, Molecular imaging of glycan chains couples cell-wall polysaccharide architecture to bacterial cell morphology, Nat. Commun. 9 (2018) 1263.
- [77] M. L. Gardel, J. H. Shin, F. C. MacKintosh, L. Mahadevan, P. Matsudaira, D. A. Weitz, Elastic behavior of cross-linked and bundled actin networks, Science 304 (2004) 1301–1305.
- [78] A. L. Koch, S. Woeste, Elasticity of the sacculus of *Escherichia coli*, J. Bacteriol. 174 (1992) 4811–4819.
- [79] T. Pilizota, J. W. Shaevitz, Fast, multiphase volume adaptation to hyperosmotic shock by *Escherichia coli*, PLoS One 7 (2012) e35205.

- [80] S. B. Zimmerman, S. O. Trach, Estimation of macromolecule concentrations and excluded volume effects for the cytoplasm of *Escherichia coli*, J. Mol. Biol. 222 (1991) 599–620.
- [81] R. J. Ellis, Macromolecular crowding: obvious but underappreciated, Trends Biochem. Sci. 26 (597–604) 2001.
- [82] J. P. Michel, Y. X. Wang, I. Kiesel, Y. Gerelli, V. Rosilio, Disruption of asymmetric lipid bilayer models mimicking the outer membrane of Gram-negative bacteria by an active plasticin, Langmuir 33 (2017) 11028–11039.
- [83] T. Abraham, S. R. Schooling, T. J. Beveridge, J. Katsaras, Monolayer film behavior of lipopolysaccharide from *Pseudomonas aeruginosa* at the air-water interface, Biomacromolecules 9 (2008) 2799–2804.
- [84] A. P. Le Brun, L. A. Clifton, C. E. Halbert, B. Lin, M. Meron, P. J. Holden, J. H. Lakey, S. A. Holt, Structural characterization of a model gram-negative bacterial surface using lipopolysaccharides from rough strains of *Escherichia coli*, Biomacromolecules 14 (2013) 2014–2022.
- [85] P. W. Fowler, J. Hélie, A. Duncan, M. Chavent, H. Kolds, M. S. P. Sansom, Membrane stiffness is modified by integral membrane proteins, Soft Mat. 12 (2016) 7792–7803.
- [86] W. Arunmanee, M. Pathania, A. S. Solovyova, A. P. Le Brun, H. Ridley, A. Baslé, B. van den Berg, J. H. Lakey, Gram-negative trimeric porins have specific LPS binding sites that are essential for porin biogenesis, Proc. Natl. Acad. Sci. USA 113 (2016) 5034–5043.
- [87] H. H. Tuson, G. K. Auer, L. D. Renner, M. Hasebe, C. Tropini, M. Salick, W. C. Crone, A. Gopinathan, K. C. Huang, D. B. Weibel, Measuring the stiffness of bacterial cells from growth rates in hydrogels of tunable elasticity, Mol. Microbiol. 84 (2012) 874– 891.
- [88] R. Buda, Y. Liu, J. Yang, S. Hegde, K. Stevenson, F. Bai, T. Pilizota, Dynamics of

Escherichia coli's passive response to a sudden decrease in external osmolarity, Proc. Natl. Acad. Sci. USA 113 (2016) 5838–5846.